Supporting Information

Ultrafine Aramid Nanofibers Prepared from High-Efficiency Wet Ball-Milling Assisted Deprotonation for High-Performance Nanopaper

Gaojie Han, Bing Zhou, Zhaoyang Li, Yuezhan Feng*, Chuntai Liu*, Changyu Shen

Key Laboratory of Materials Processing and Mold Ministry of Education, National Engineering Research Center for Advanced Polymer Processing Technology, Zhengzhou University, Zhengzhou 450002, China.

*Corresponding Author,

E-mail: yzfeng@zzu.edu.cn (Y. Feng), ctliu@zzu.edu.cn (C. Liu)

Experimental section:

Preparation of the control ANF solutions

The ANF-MS solution was prepared by traditional magnetic stirring (MS) to achieve the deprotonation of macroscopic Kevlar fibers. Typically, 1 g Kevlar fibers and 1.5 g KOH were added to 500 mL DMSO and magnetically stirred for 7 days at room temperature, followed by centrifuged at 8,000 rpm for 5 min to form a dark-red ANF-MS dispersion (Fig. S1a).

The preparation of ANF/H_2O-MS solution was based on magnetic stirring assisted by proton donor. Typically, 1 g Kevlar fibers and 1.5 g KOH were added to the mixture of 500 mL DMSO and DI H_2O with different ratios, and magnetically stirred to form ANF at room temperature (Fig. S1b). The judging endpoint of the Kevlar fibers deprotonation process was that the split macroscopic fibers were invisible under a polarized-light optical microscopy (POM).

The ANF-BM solution was prepared by ball milling-assisted deprotonation process without proton donor. In a typical process, 1g Kevlar fibers and 1.5g KOH were first added into a 250 mL zirconia tank with 100 mL DMSO, then zircite balls (diameter: 10/5/2 mm = 50/120/70 g) were added into tank with stirring manually for 1 min to mix well. The mixture was ball-milled at a rotation speed of 400 rpm by using a planetary ball mill, and the POM was used to determine the endpoint of the protonation reaction (Fig. S1c).

Preparation of ANF hydrogel/aerogel fibers

A wet spinning method was used to prepare ANF hydrogel/aerogel fibers. Typically,

the obtained ANF solutions (1 wt%) was extruded from a pump-controlled syringe at a rate of 3 mL/h into a coagulation bath (5% CH_3COOH aqueous); here, the continuous hydrogel fibers were immediately formed though solvent replacement. The ANF hydrogel fibers were fabricated after washing away the residual coagulation solution, The hydrogel fibers were directly freeze-dried in a freeze-drier at -50 °C for 48 h for to obtain ANF aerogel fibers. ANF hydrogel fibers were dried at 60 °C for 10 h to prepare ANF fibers.

Preparation of 3D ANF skeletons

ANF skeletons were prepared via unidirectional freezing process. Firstly, a certain amount of ANF solutions (1 wt%) was first diluted to 0.5 wt% by adding DMSO with stirring for 30 min. Subsequently, the obtained ANF solutions were poured into a Teflon mold, and unidirectional freeze casting was conducted by placing the mold on a copper column, which was cooled by liquid nitrogen. Finally, ANF skeletons were obtained in a freeze-dryer (–50°C, <10 Pa) for 72 h.

Characterization:

The split-peak fitting software and procedure of XPS.

The software used for the split-peak fitting of XPS is *XPSPEAK41*, the fitting function is based on the Lorentzian-Gaussian function. The procedure mainly includes the following 6 steps:

(1) Convert each element data (binding energy and spectral line intensity) to txt format;

(2) Import txt files using *XPSPEAK41* software;

(3) Establishing a baseline, *i.e.* click on Background in the menu;

(4) Click Add peak and a new window will pop up, select s, p, d, f etc. peak types from Peak Type;

(5) Manual correction. On this basis, manually adjust the peak area, full width at half

maximum (FWHM) and other parameters to make the fitted data coincide with the raw data as much as possible;

(6) Save and export the fitted data. After the fitting is finished, click Save XPS in XPS peak processing to store the fitting results as .xps files.

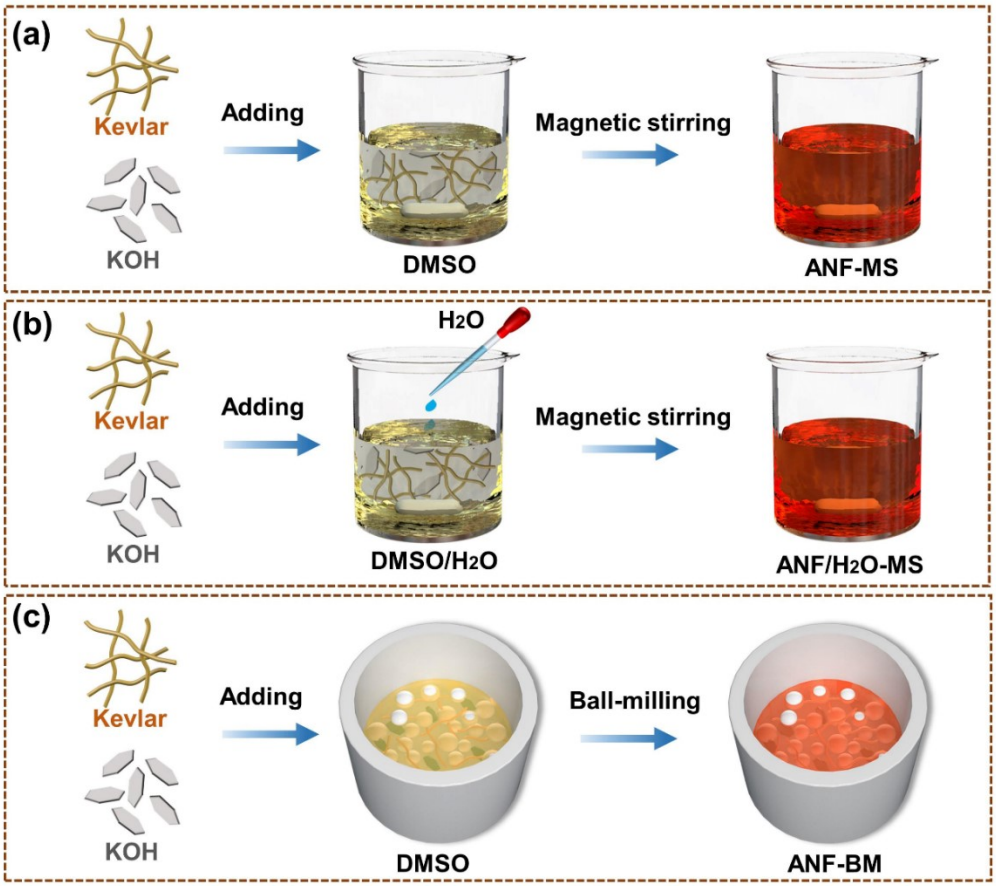

Fig. S1. Schematic illustration of the preparation of ANF through (a) magnetic stirring, (b) magnetic stirring assisted by proton donor, and (c) ball-milling without proton donor.

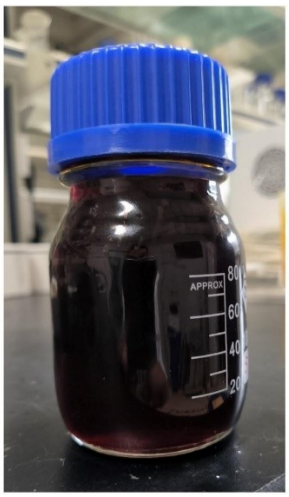

Fig. S2. Scale-up preparation of ANF from the macroscopical Kevlar aramid fibers.

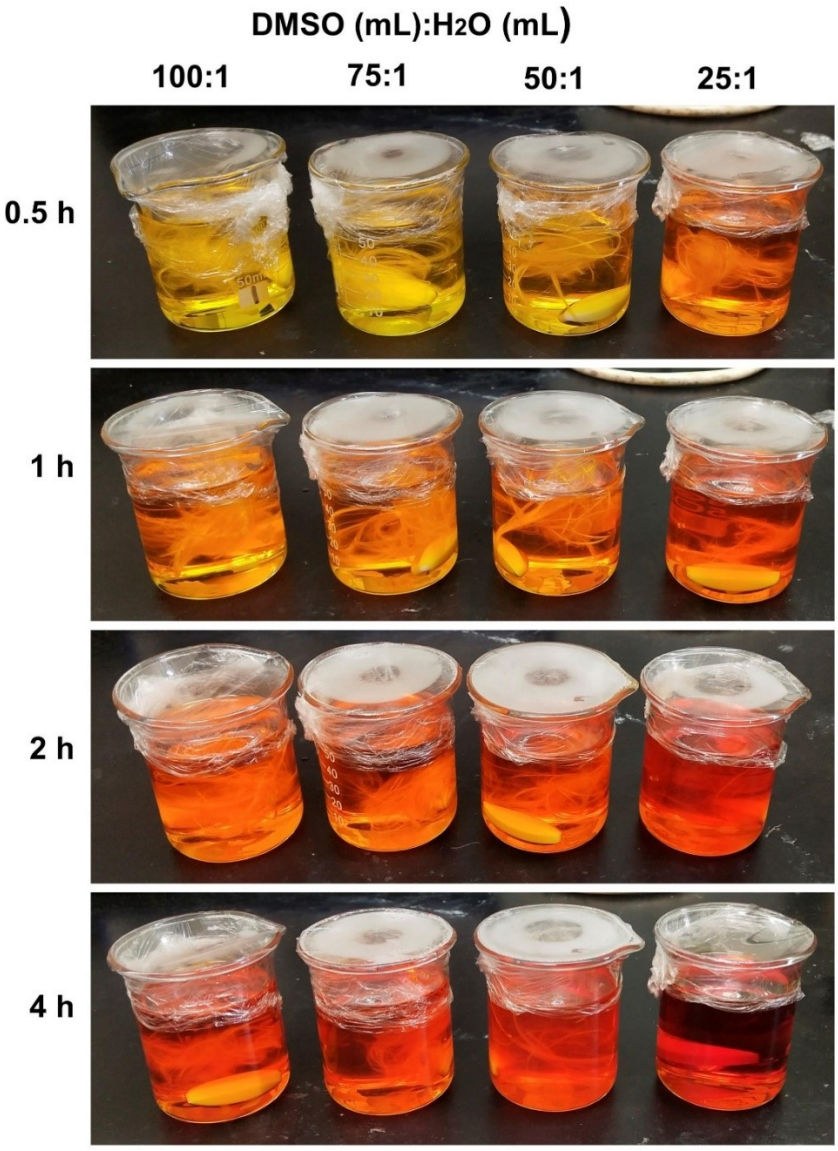

Fig. S3. Digital photos of the ANF/H_2O-MS with varying volumes of water and stirring times.

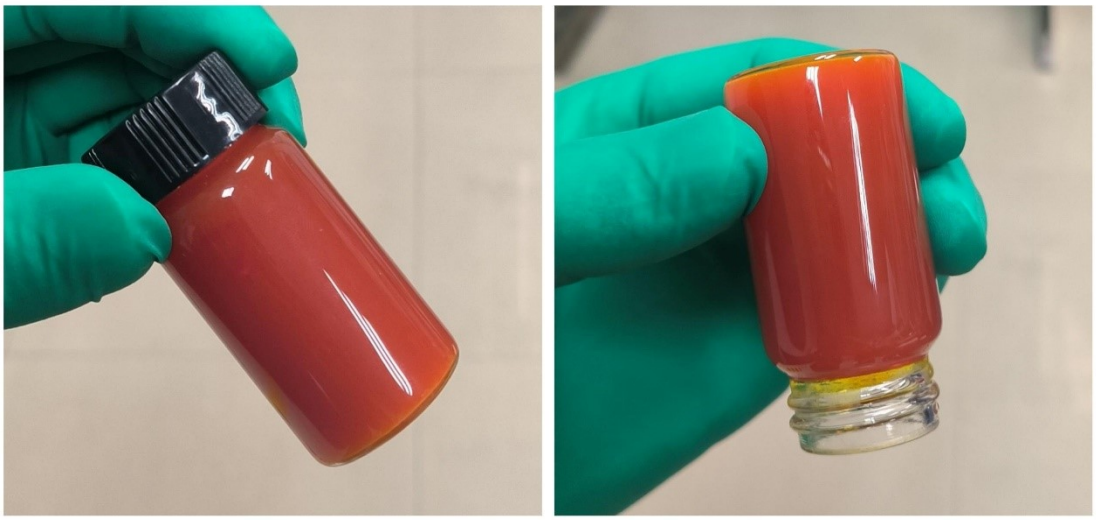

Fig. S4. Digital photo of high concentration ANF/H_2O-BM (4 wt%).

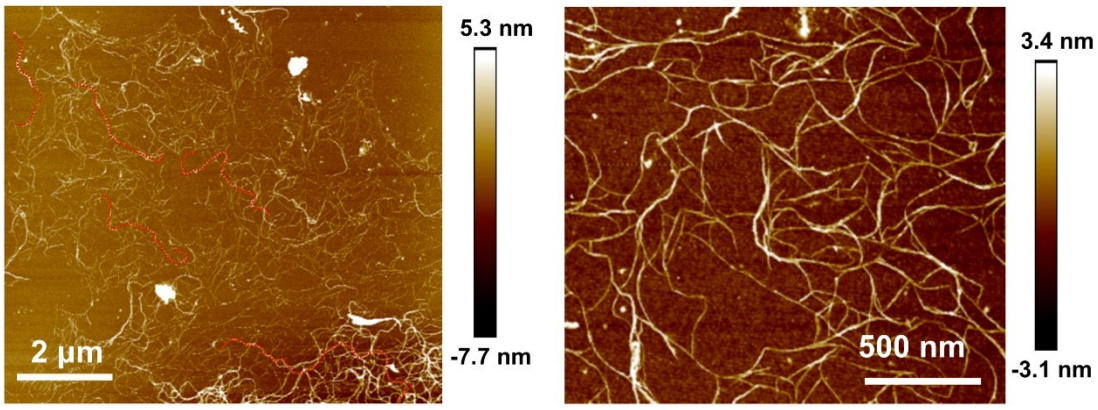

Fig. S5. AFM images of ANF/H_2O-BM.

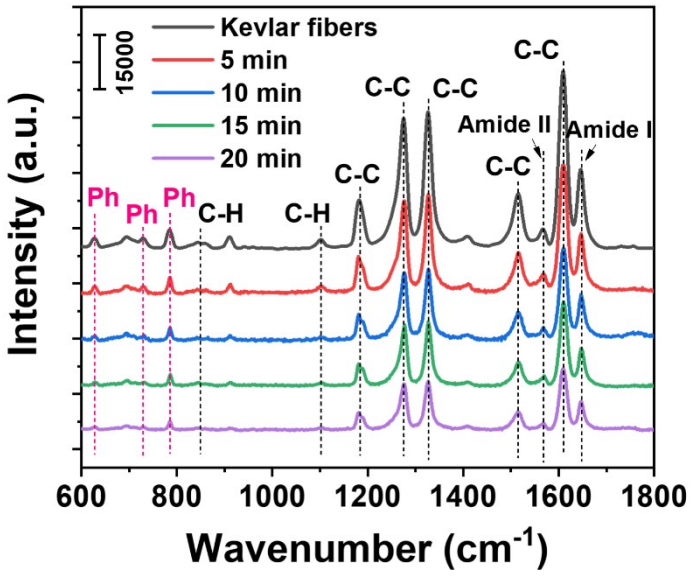

Fig. S6. Raman scattering of extracting Kevlar fibers with different ball-milling time.

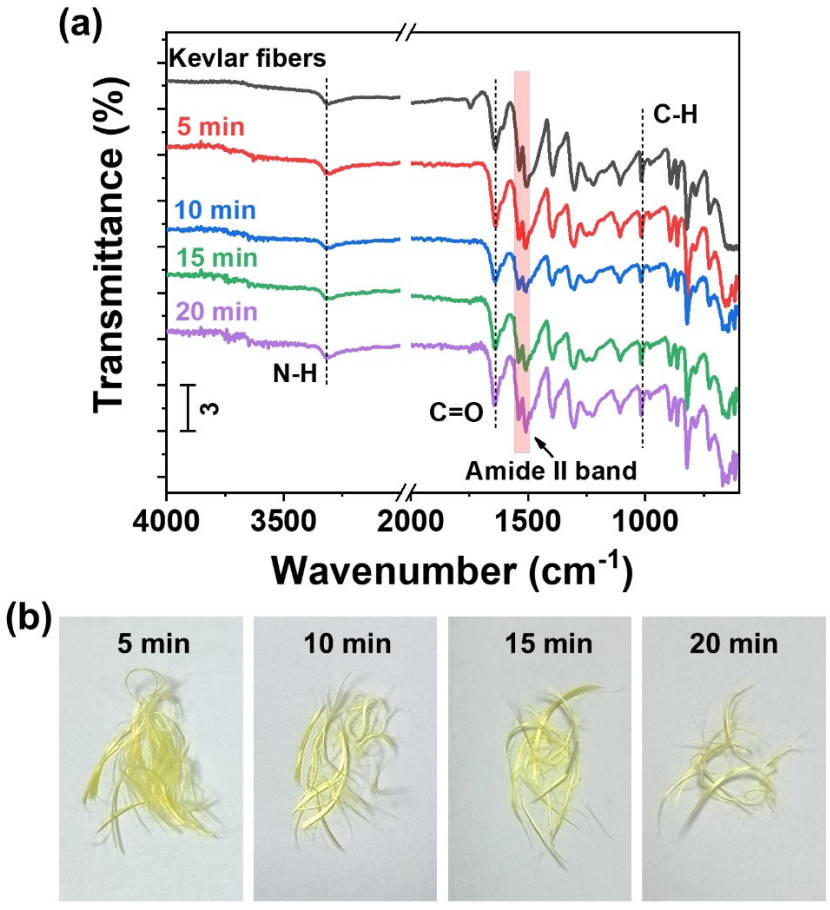

Fig. S7. (a) FTIR spectra of extracting Kevlar fibers with different ball-milling time.

(b) Photographs of extracting Kevlar fibers during BMAD process.

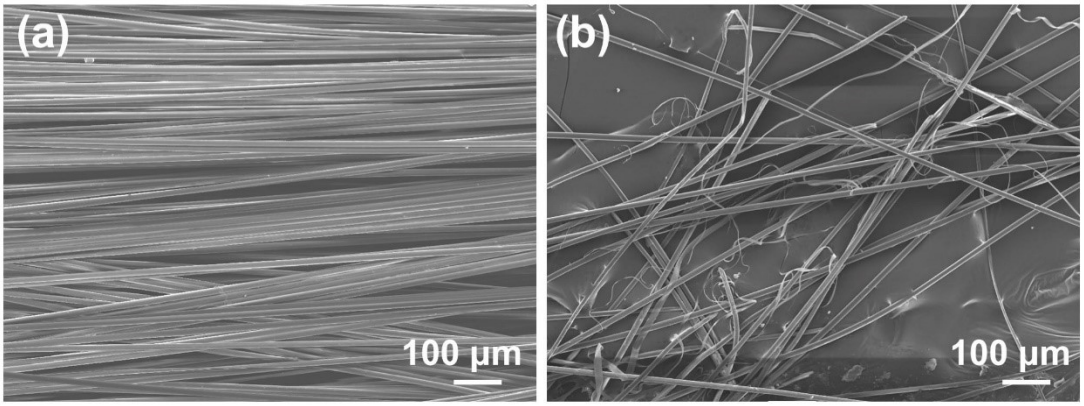

Fig. S8. SEM images of (a) pristine Kevlar fibers and (b) extracting micro-fibers bundles during the BMAD process.

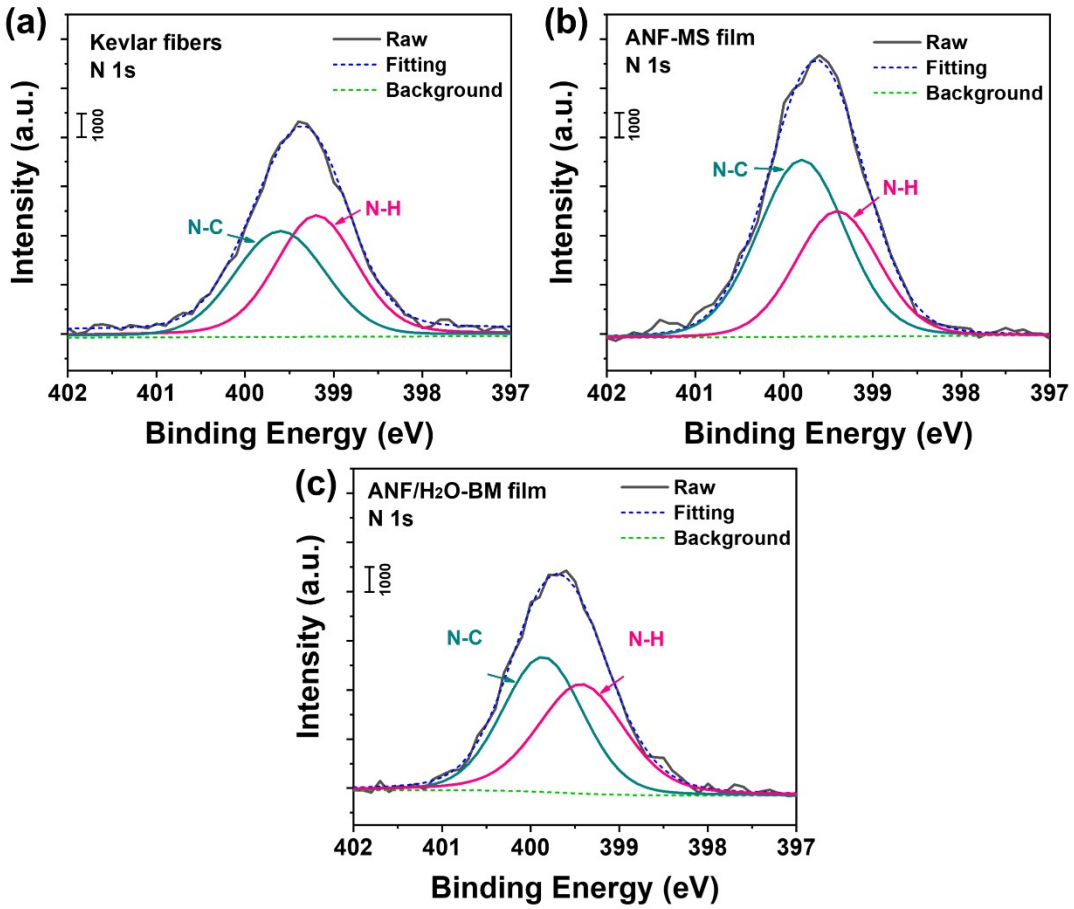

Fig. S9. High-resolution XPS analysis of N 1s: (a) Kevlar fibers, (b) ANF-MS and (c) ANF/H_2O-BM nanopapers.

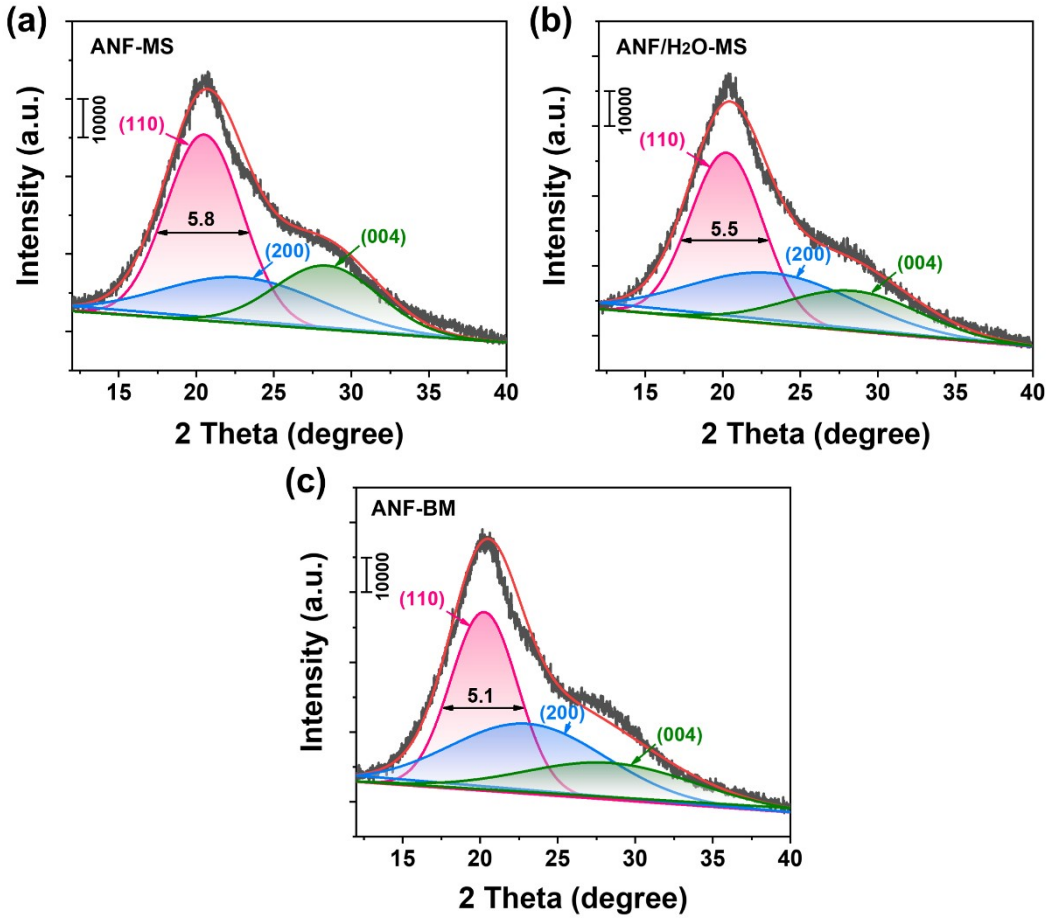

Fig. S10. Fitting peaks of XRD patterns of (a) ANF-MS, (b) ANF/H_2O-MS, (c) ANF-BM nanopapers.

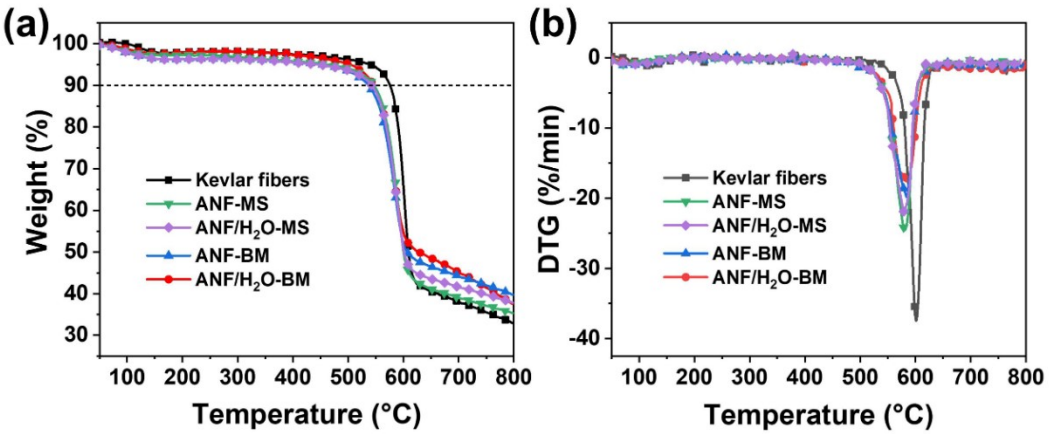

Fig. S11. (a) TGA and (b) DTG curves of different ANF nanopapers under N_2 atmosphere.

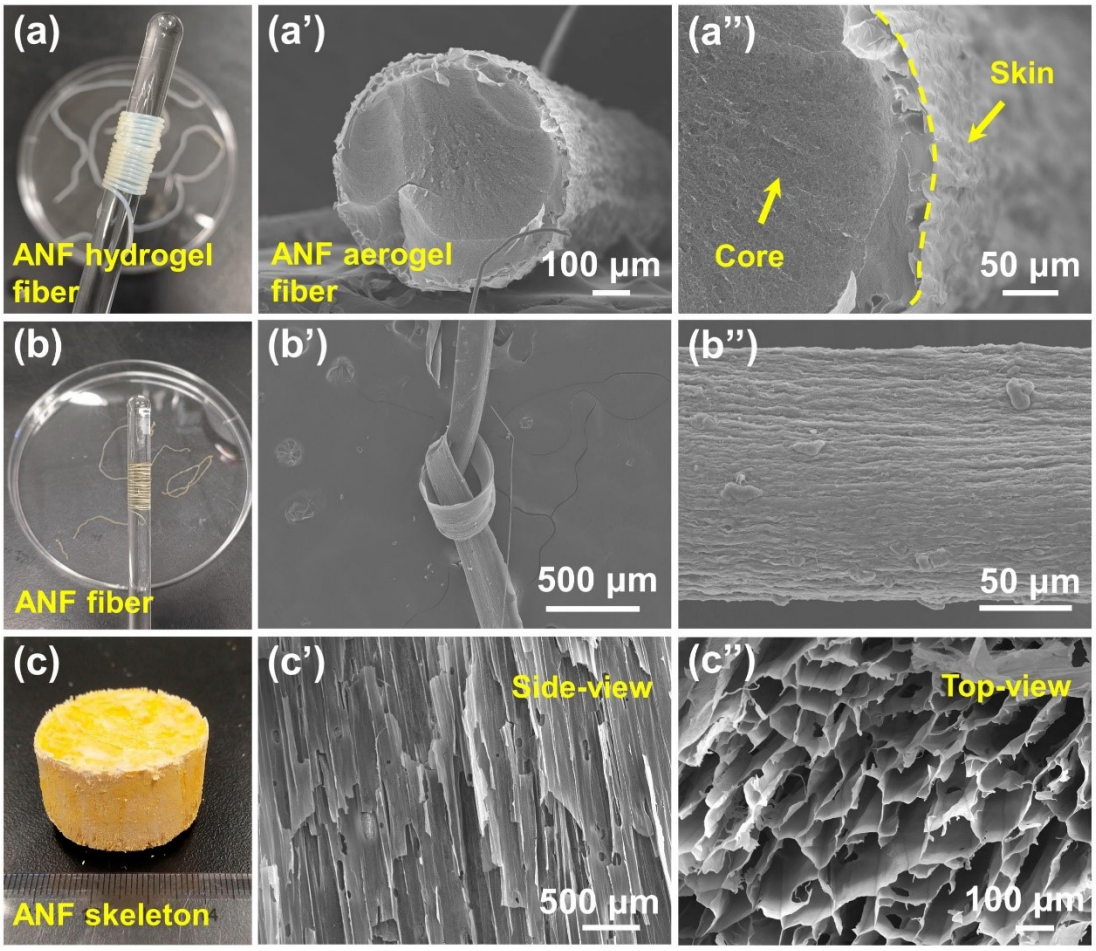

Fig. S12. Fabrication and morphologies of ANF-based materials. Photographs of (a) ANF hydrogel fiber, (b)ANF fiber, and (c) ANF skeleton. SEM images of (a', a'') ANF aerogel fiber, (b', b'') ANF fiber, (c') side-view and (c'') top-view for ANF skeleton.

As shown in Fig. S12a, the ANF hydrogel fibers were continuously prepared by a wet spinning technology comprising a sol-gel transformation and solvent exchange process. It can be clearly seen that the ANF hydrogel fibers present a light yellow due to rapidly reprotonation process in deionized (DI) water. Notably, the microstructure of ANF hydrogel fibers could be tailored by controlling technological parameters including the concentration of ANF dispersion, reprotonation time in coagulation bath, proton acid type and draft ratio, etc. The corresponding ANF aerogel fibers can be

directly prepared by freeze-drying at -50 °C. SEM images revealed continuous and uniform 3D network structure with a dense surface layer and a porous internal structure (Fig. S12a'-a''). The phenomenon is a clear manifestation of the outermost ANF was rapidly reprotonated to form a several-nm-thick skin layer when ANF/DMSO entered the coagulation bath. This unique asymmetric structure also be used in the preparation of ANF-based sol-gel membranes for energy-saving and thermal protection applications. In addition, the corresponding ANF fibers can be achieved after drying the prepared hydrogel fibers in a vacuum oven at 60 °C (Fig. S12b). As shown in Fig. S12b' and b'', the ANF fibers possess high flexibility allows them to be knotted without breaking, while their surface produces a pleated structure due to width shrinkage of the ANF hydrogel fibers. As one of the most important components of wearable electronic systems, flexible fibers or wires have shown great potential due to their ease of mass production and can be woven into textiles. Besides, ANF skeleton with 3D aligned networks was obtained by unidirectional freezing and freeze-drying process (Fig. S12c). The morphology of ANF skeleton in the horizontal and vertical directions were detailedly investigated by SEM, showing a well long-range continuous cellular structure with uniform pore channels (Fig. S12c' and c''). As a polymeric "binders" with high adhesion, large specific surface area and high porosity, ANF framework can serve as the next-generation thermal insulation materials.

Table S1. Comparison of Preparation time of ANF between different methods.

Preparation method	Concentration (wt%)	Preparation time (h)	Efficiency (g L^{-1} h^{-1})	Diameter (nm)	Refs.
Polymerization induced self-assembly	3	--	--	20-50	[1]
Electrospinning	--	>24	--	275-15000	[2]
Deprotonation (DMSO/KOH)	0.2	168	0.012	10±3	[3]
Deprotonation (DMSO/KOH)	0.3	168	0.018	30-40	[4]
Deprotonation (DMSO/KOH)	0.4	168	0.024	30-40	[5]
Deprotonation (DMSO/KOH)	1	168	0.06	5-10	[6]
Deprotonation (DMSO/KOH)	1.25	168	0.074	3-14	[7]
Deprotonation (DMSO/t-BuOK)	0.5	168	0.03	9-18	[8]
Deprotonation (DMSO/EtOK)	1	168	0.06	2-9	[9]
Fibrillation-assisted deprotonation	0.2	72	0.028	12-17	[10]
Ultrasonication-assisted deprotonation	0.2	24	0.083	10-14	[10]
Proton donor-assisted deprotonation	0.2	4	0.5	10-12	[10]

Deprotonation (DMSO/KOH(aq))	0.2	0.48	4.167	8-12	[11]
BMAD approach (DMSO/KOH)	0.2	<2	>1	2-5.5	**This work**
BMAD approach (DMSO/KOH/H_2O)	1	0.5	20	1-4	**This work**

Table S2. TGA and DTG data of ANF nanopapers.

Sample	$T_{10\ wt\%}$ (°C)	T_{max} (°C)	Char at 700 °C (wt%)
Kevlar fibers	575.3	601.2	38.0
ANF-MS	542.1	581.7	39.1
ANF/H_2O-MS	543.6	581.4	41.5
ANF-BM	547.2	584.3	44.1
ANF/H_2O-BM	548.5	586.2	44.9

$T_{10\ wt\%}$ is defined as the temperature of 10 wt% weight loss in TGA curve. Maximum degradation temperature (T_{max}) is evaluated by the peak in DTG curves.

Table S3. Mechanical properties of ANF nanopapers.

Samples	Stress (MPa)	Elongation at break (%)	Young's modulus (GPa)	Toughness (MJ/m^3)
ANF-MS	191.5±16	11.9±1	3.16±0.18	14.7±1.2
ANF/H_2O-MS	199.2±18	13.2±1.1	3.09±0.2	16.4±1.6
ANF-BM	221.1±12	15.6±0.8	4.23±0.16	21.4±1.1
ANF/H_2O-BM	271.7±10	20.1±0.6	4.16±0.14	33.1±0.9

Table S4. Comparison of mechanical properties between the ANF/H_2O-BM nanopapers and other reported materials.

Sample	Material name	Stress (MPa)	Strain (%)	Toughness (MJ/m^3)	Refs.
1	F-30000 r ANF film	109.9	5.9	--	[10]
2	UL-120 min ANF film	118.9	7.1	--	[10]
3	PD-1:25 ANF film	164.5	8.3	--	[10]
4	ANFs/PEO separator	41.52	15.5	--	[12]
5	Cellulose/ANFs film	54.4	15.8	6.10	[13]
6	HAP/ANF paper	73.5	7.4	3.58	[14]
7	ANF film (fabric fiber)	149.2	10.4	10.43	[15]

8	LM/ANF film	108.5	17.8	10.3	[16]
9	ANF film	157.4	17.1	17.1	[17]
10	ANF/MXene-PEDOT:PSS Janus film	155.9	20	19.4	[17]
11	ANF membrane	92	3.7	--	[3]
12	MXene/ANF paper	198.8	15.3	21.87	[18]
13	MXene/ANF membrane	101	4.65	2.64	[6]
14	ANF/BNNS film	167	5.64	6.16	[19]
15	BNNS@PDA/ANF paper	67.5	18	--	[5]
16	CuNWs/ANF nanopaper	228	3.8	0.42	[20]
17	BNNS-M/PBO paper	206	7.01	--	[21]
18	CNF film	118.5	5.2	3.9	[22]
19	CNF@MXene film	112.5	4.3	2.7	[22]
20	d-$Ti_3C_2T_x$/CNF paper	135.4	16.7	14.8	[23]
21	CNC/CNF film	151.6	2.68	2.72	[24]
22	ANF/-BM (BMAD)	221.1	15.6	21.4	**This work**
23	ANF/H_2O-BM (BMAD)	271.7	20.1	33.1	**This work**

References

1. H. Yan, J. Li, W. Tian, L. He, X. Tuo and T. Qiu, *RSC Adv.*, 2016, **6**, 26599-26605.
2. J. Yao, J. Jin, E. Lepore, N. M. Pugno, C. W. M. Bastiaansen and T. Peijs, *Macro. Mater. Eng.*, 2015, **300**, 1238-1245.
3. C. Chen, G. Yang, D. Liu, X. Wang, N. A. Kotov and W. Lei, *Adv. Funct. Mater.*, 2022, **32**, 2102080.
4. S. R. Kwon, J. Harris, T. Zhou, D. Loufakis, J. G. Boyd and J. L. Lutkenhaus, *ACS Nano*, 2017, **11**, 6682-6690.
5. T. Ma, Y. Zhao, K. Ruan, X. Liu, J. Zhang, Y. Guo, X. Yang, J. Kong and J. Gu, *ACS Appl. Mater. Interfaces*, 2020, **12**, 1677-1686.
6. Z. Zhang, S. Yang, P. Zhang, J. Zhang, G. Chen and X. Feng, *Nat. Commun.*, 2019, **10**, 2920.
7. J. Gao, G. Han, J. Song, C. He, J. Hu, W. Wang, Y. Feng and C. Liu, *Mater. Today Phys.*, 2022, **27**, 100811.
8. S. Hu, S. Lin, Y. Tu, J. Hu, Y. Wu, G. Liu, F. Li, F. Yu and T. Jiang, *J. Mater. Chem. A*, 2016, **4**, 3513-3526.
9. J. Zhu, M. Yang, A. Emre, J. H. Bahng, L. Xu, J. Yeom, B. Yeom, Y. Kim, K. Johnson, P. Green and N. A. Kotov, *Angew. Chem. Int. Ed.*, 2017, **56**, 11744-11748.
10. B. Yang, L. Wang, M. Zhang, J. Luo and X. Ding, *ACS Nano*, 2019, **13**, 7886-7897.
11. H. J. Chen, Q. Y. Bai, M. C. Liu, G. Wu and Y. Z. Wang, *Green Chem.*, 2021, **23**, 7646-7658.

12. W. Tang, Q. Liu, N. Luo, F. Chen and Q. Fu, *Compos. Sci. Technol.*, 2022, **225**, 109479.

13. G. Xia, Q. Zhou, Z. Xu, J. Zhang, J. Zhang, J. Wang, J. You, Y. Wang and H. Nawaz, *Carbohydr. Polym.*, 2021, **273**, 118569.

14. Z. Y. Wang, Y. J. Zhu, Y. Q. Chen, H. P. Yu and Z. C. Xiong, *Chem. Eng. J.*, 2022, **444**, 136470.

15. B. Yang, W. Li, M. Zhang, L. Wang and X. Ding, *ACS Nano*, 2021, **15**, 7195-7207.

16. L. C. Jia, Y. F. Jin, J. W. Ren, L. H. Zhao, D. X. Yan and Z. M. Li, *J. Mater. Chem. C*, 2021, **9**, 2904-2911.

17. B. Zhou, J. Song, B. Wang, Y. Feng, C. Liu and C. Shen, *Nano Research*, 2022, **15**, 9520-9530.

18. J. Wang, X. Ma, J. Zhou, F. Du and C. Teng, *ACS Nano*, 2022, **16**, 6700-6711.

19. K. Wu, J. Wang, D. Liu, C. Lei, D. Liu, W. Lei and Q. Fu, *Adv. Mater.*, 2020, **32**, 1906939.

20. T. T. V. Tran, V. A. Le, C. H. Nguyen, D. V. N. Vo, T. M. Nguyen, C. Samart, S. Kongparakul, S. Ghotekar and C. M. Vu, *ACS Appl. Nano Mater.*, 2022, **5**, 12991-13001.

21. Y. Chen, H. Zhang, J. Chen, Y. Guo, P. Jiang, F. Gao, H. Bao and X. Huang, *ACS Nano*, 2022, **16**, 14323-14333.

22. B. Zhou, Z. Zhang, Y. Li, G. Han, Y. Feng, B. Wang, D. Zhang, J. Ma and C. Liu, *ACS Appl. Mater. Interfaces*, 2020, **12**, 4895-4905.

23. W. T. Cao, F. F. Chen, Y. J. Zhu, Y. G. Zhang, Y. Y. Jiang, M. G. Ma and F. Chen, *ACS Nano*, 2018, **12**, 4583-4593.

24. X. Zhang, R. Xiong, S. Kang, Y. Yang and V. V. Tsukruk, *ACS Nano*, 2020, **14**, 14675-14685.